Evolution of Fermi-liquid behavior with doping in the Hubbard model: Influence of the band structure

Jungsoo Kim and D. Coffey
Department of Physics, State University of New York, Buffalo, New York 14260
(Received 21 December 1999; revised manuscript received 5 April 2000)

We calculate the single-particle Green's function for a contact interaction with nearest-neighbor hopping on a square lattice as a function of chemical potential μ. This allows us to investigate the dependence of the leading Fermi-liquid dependencies on the band structure as the Fermi surface evolves from a circle at $\mu \sim -4t$ to a square at $\mu=0$. The form of the single-particle self-energy $\Sigma(\vec{p},E)$ is determined by the density-density correlation function $\chi(\vec{q},\omega)$ which develops two peaks for $\mu \gtrsim -2.5t$ unlike the parabolic band case. Near half-filling, $\chi(\vec{q},\omega)$ becomes independent of ω, one-dimensional behavior, at intermediate values of ω, which leads to the one-dimensional behavior in $\Sigma(\vec{p},E)$. However, with $\mu \lesssim -0.1t$ there is no influence on the Fermi-liquid dependencies from the spin-density wave instability. We find that throughout the doping region $\Sigma(\vec{p},E)$ remains qualitatively the same as for the isotropic Fermi surface with quantitative differences. The strong $\vec{p}$ and E dependence of the off-shell self-energy $\Sigma(p,E)$ found earlier for the parabolic band is recovered for $\mu \lesssim -t$ but deviates from this develop for $\mu \gtrsim -0.1t$. The resonance peak width of the spectral function $A(\vec{p}E)$, has a linear dependence in $\xi_{\vec{p}}$ due to the E dependence of the imaginary part of $\Sigma(\vec{p},E)$. We point out that an accurate detailed form for $\Sigma(\vec{p},E)$ would be very difficult to recover from angle-resolved photoemission spectroscopy data for the spectral density. Since the leading corrections are determined by the long wavelength particle-hole excitations, the results found here for the Hubbard model carry over to Hamiltonians with finite range interactions.

I. INTRODUCTION

The Fermi-liquid (FL) theory has been used to describe the metallic phase in which the quasiparticle concept develops from a free-electron model to study the metallic behavior.[1] Since the discovery of high-temperature superconductivity in the cuprates,[2] the normal state properties of the quasi-two-dimensional cuprates have been investigated experimentally and theoretically. The experimental observations such as optical conductivity,[3] electrical resistivity,[4–6] and angle-resolved photoemission spectroscopy (ARPES)[7,8] do not follow the conventional FL behaviors. The absence of those FL dependencies has lead to a proposal that the FL model for these quasi-low-dimensional conductors should be discarded in favor of a Luttinger liquid-like model[9] in which there is a separation of charge and spin degrees of freedom in the elementary excitation.

However Castellani *et al.* have shown that the FL regime is recovered for dimensions greater than one, having investigated the instability of Luttinger liquid (LL) by analyzing correlated fermions with anisotropic hopping amplitudes in a one-dimensional system[10] and dimensional crossover from FL to LL using analytic continuation for noninteger dimensions.[11] Independent calculations show that arbitrarily small transverse hopping kills off LL.[12,13] They also found no breakdown of the perturbation theory.

Given that the expected FL dependencies are based on parabolic band (a spherical Fermi surface model) and a quasiparticle approximation and assuming that the ground state is analytically continuous to the noninteracting ground state as a function of interaction strength, the discrepancy between the FL picture and the experiment has two possibilities. Firstly the conventional FL dependencies are present but they are limited to anomalously low energy and the temperature scales induced by interactions among the fermions or by the band structure of the noninteracting fermions. In this picture the spectral density of the single-particle Green's function is still characterized by a single-particlelike sharp resonance for momenta very close to the Fermi surface whose width becomes progressively broader as the quasiparticle momenta move further from the Fermi surface where the quasiparticle approximation breaks down. The second possibility can be viewed as an extreme case of the first possibility in which the interactions are so strong that the quasiparticle approximation breaks down over at least some region of the Fermi surface. In this case the ground state is still a FL in that it has developed analytically out of the noninteracting ground state. This picture is supported by ARPES measurements[14,15] on the underdoped cuprates although the quasiparticle peaks remain anomalously broad at the chemical potential.[16] In these experiments the Fermi surface seems to develop around a particular direction, signaled by a quasiparticle peak in the measured spectral density at low doping. The region in which there is a Fermi surface defined by the vanishing of a quasiparticle peak grows with doping until the whole surface is established.[8] The absence of a quasiparticle peak is referred to as a pseudogap. Previously this type of data for underdoped cuprates had been described in terms of hole pockets that were shown to arise from strong correlation effects in calculations of the t-J model.[17–20] However a search for these pockets in the recent ARPES results[8] was unsuccessful.

The leading two-dimensional (2D) FL behavior for the on-shell self-energy with an isotropic band structure at zero

temperature $\xi_{\vec{p}}=\vec{p}^2/2m-p_f^2/2m$ is

$$\Sigma'(\vec{p},\xi_{\vec{p}})=-\alpha\xi_{\vec{p}}-\frac{\pi}{2}\beta\xi_{\vec{p}}|\xi_{\vec{p}}|-\gamma|\xi_{\vec{p}}|^{5/2}+O(\xi_{\vec{p}}^3), \quad (1a)$$

$$\Sigma''(\vec{p},\xi_{\vec{p}})=\beta\xi_{\vec{p}}^2\ln|\xi_{\vec{p}}/\xi_0|+O(\xi_{\vec{p}}^4), \quad (1b)$$

where the cut-off energy ξ_0 is isotropic.[21] This form for $\Sigma(\vec{p},E)$ is generic for 2D Fermi liquids and is independent of the details of the interaction term in the Hamiltonian. In particular β depends only on long wavelength properties of the interaction among the quasiparticles. These leading on-shell dependencies of the imaginary part of the self-energy had been determined previously by a number of authors.[22,23] For low-density system ξ_0 goes to zero so that the region of the generic Fermi-liquid behavior is limited. The $\xi_{\vec{p}}|\xi_{\vec{p}}|$ energy dependence in the real part is a mirror of the imaginary part of the self-energy $\beta\xi_{\vec{p}}^2\ln\xi_{\vec{p}}$ through the Kramers-Kronig relation, which gives a T^2 contribution to the specific heat in addition to that from zero sound.[24] The $|\xi_{\vec{p}}|^{5/2}$ term is the leading zero-sound contribution. This term has a corresponding $(\xi_{\vec{p}}-\xi_{th})^{3/2}$ term in $\Sigma''(\vec{p},\xi_{\vec{p}})$, where $\xi_{th}=(v_{zs}-v_f)p_f$, determined by the velocity of the zero-sound mode. The 2D calculation for a parabolic band shows no evidence of a breakdown in FL theory and is similar to the 3D case. The cut-off energy ξ_0 has a corresponding cut-off temperature T_0, which restricts the leading correction to the FL behavior in $\Sigma''(p,\xi_p,T)$ so that T behavior will take over the FL behavior at low-density limit.[21] These cutoffs are determined by the quasiparticle interactions and the characteristic energy of the noninteracting system E_f.

As the system goes to quasi-1D band, which can be modeled by considering different ratios of t_x and t_y, for example, quasi-1D organic materials such as $(TMTSF)_2X$ or $BEDT\text{-}TTF$,[25] the van Hove singularity moves to the bottom of the band so that particle-hole (ph) pair contribution is more important than particle-particle (pp) contribution for the low-density limit. In this case the nature of the q1D FL behavior remains similar to that of the 2D FL.[26] For the parabolic band structure, the pp channel, which leads to the Cooper instability, is more important than the ph channel in 3D and vice versa in 1D due to the density-of-states. No particular set of diagrams is significant in 2D,[27] but at least the second-order calculation is shared by both channels so that the functional dependence in either one will represent the FL behavior. The pp channel is discussed later in this paper.

The cuprates have an anisotropic band structure that can lead to strong band-structure features in the density-of-states. This anisotropy of the band structure is used in a number of different models to explain the lack of the FL dependencies in experiment.[28,29] The anisotropy has been invoked to describe transport data in the hot spot[30] and cold spot[31] models. In the hot spot model, it is proximity to the SDW instability that is important whereas in the cold spot model it is proximity to the superconducting phase through pairing fluctuations that leads to the anisotropy. More recently renormalization-group calculations have shown that if the Fermi surface is dominated by a set of saddle points in the density-of-states, the Landau FL theory, the quasiparticle approximation to FL theory, can breakdown.[32]

The Hubbard model has been employed extensively in theoretical investigations of the normal state properties of the cuprates because the tight-binding band structure and the short-range Coulomb correlations result in an effective magnetic Hamiltonian for low doping, which is consistent with the data. We investigate the FL characteristics of this model as a function of chemical potential μ from $\mu=-3t$, where the Fermi surface is a circle, to $\mu=-0.1t$, near half-filling, where it is almost a square. A 2D nearest-neighbor tight-binding band structure $\xi_{\vec{p}}=-2t\cos p_x-2t\cos p_y-\mu$ will be used to determine the momentum and energy dependence of the single-particle properties in the FL behavior where t is the nearest-neighbor hopping constant. Near the half-filling, curved $\overline{M}$ points are connected by flat Fermi surface, which is a good model for the band structure of $Bi_2Sr_2CaCu_2O_8$ in which there is a strongly nested vector.[33] The Hamiltonian includes a repulsive contact interaction that we treat in the weak-coupling approximation. By introducing a cutoff q_c for the interaction in the calculation, the influence of the long wavelength interactions on $\Sigma(\vec{p},E)$ in the ph channel has been investigated in this model and shown to determine the functional form of $\Sigma(\vec{p},E)$ at low energies as in the parabolic band case. The evolution of the leading behaviors in the real and imaginary part is determined by the changes in the bare ph propagator as the Fermi surface becomes more anisotropic. First we calculate the contribution to $\Sigma(\vec{p},\xi_{\vec{p}})$, the on-shell self-energy, to the second order in the interaction that gives the functional form of the corrections and then consider the effect of the repeated scattering from the ph channel, which would indicate the influence of any instabilities in these behaviors.

We next calculate the off-shell self-energy $\Sigma(\vec{p},E)$, which is probed directly in angle-resolved photoemission through the spectral density $A(\vec{p},E)$. It is found that the energy dependence of the imaginary part of $\Sigma(\vec{p},E)$ leads to a width of the quasiparticle resonance in $A(\vec{p},E)$ which is linear in $\xi_{\vec{p}}$ even when the on-shell $\Sigma''(\vec{p},E)$ has the expected $\xi_{\vec{p}}^2\ln\xi_{\vec{p}}$ dependence. Some authors have pointed to this linear dependence in $\xi_{\vec{p}}$ as evidence for non-Fermi liquid character in the normal state properties of the cuprates. We point to the difficulty of extracting the functional form of off-shell self-energy from ARPES data on the spectral function.

II. CALCULATIONS

The form of the Hamiltonian is

$$H=\sum_{\vec{p},\sigma}\xi_{\vec{p}}c_{\vec{p},\sigma}^{\dagger}c_{\vec{p},\sigma}+\sum_{\vec{p},\vec{p}',\vec{q},\sigma,\sigma'}Uc_{\vec{p},\sigma}^{\dagger}c_{\vec{p}',\sigma'}c_{\vec{p}'-\vec{q},\sigma'}^{\dagger}c_{\vec{p}+\vec{q},\sigma}, \quad (2)$$

where $\xi_{\vec{p}}=-2t\cos p_x-2t\cos p_y-\mu$ is the electronic band structure and U is the electron-electron interaction that is treated as a perturbation term. The single-particle self-energy, $\Sigma(\vec{p},E)=\Sigma'(\vec{p},E)+i\Sigma''(\vec{p},E)$ is given by

$$\Sigma(\vec{p},iE_n)=-T\sum_{\vec{q},\omega_l} G(\vec{p}-\vec{q},iE_n-i\omega_l)U_{eff}(\vec{q},i\omega_n), \tag{3}$$

where $G(\vec{p},iE_n)$ is the unperturbed temperature Green's function and ω_l are the Bose Matsubara frequencies. The U_{eff} includes all the ph diagrams in principle. As a function of filling the electronic band structure develops an anisotropic Fermi surface that will end up with the quasi-one-dimensional square Fermi surface at $\mu=0$. As the system goes to half-filling, the density-of-states at the Fermi surface approaches the van Hove singularity, which makes the ph channel more significant in the low-filling system. We concentrate on two directions in momentum space throughout the calculations, $(1,0)p$ and $(1,1)p$, which are the extreme directions in the tight-binding band structure.

The accurate calculation of the density-density correlation function is essential in this study. The correlation function $\chi(\vec{q},\omega)=\chi'(\vec{q},\omega)+i\chi''(\vec{q},\omega)$ for the ph channel is given by

$$\chi(\vec{q},\omega)=\sum_{\vec{p}} \frac{f(\xi_{\vec{p}+\vec{q}})-f(\xi_{\vec{p}})}{\omega-(\xi_{\vec{p}+\vec{q}}-\xi_{\vec{p}})}. \tag{4}$$

The imaginary part of the density-density correlation function for the tight-binding band structure is given by

$$\chi''(\vec{q},\omega>0)=\frac{1}{4\pi}\int dp_x \int dp_y \frac{\Theta(\xi_{\vec{p}})\Theta(-\xi_{\vec{p}-\vec{q}})\delta(p_y-p_y^*)}{|-4t\sqrt{\sin^2 q_y/2-[\omega/4t-\sin(p_x-q_x/2)\sin q_x/2]^2}|} \tag{5a}$$

$$p_y^*=\sin^{-1}\left[\frac{\omega-4t\sin(p_x-q_x/2)\sin q_x/2}{4t\sin q_x/2}\right]+\frac{q_y}{2} \tag{5b}$$

in which subscripts x and y can be switched when $q_y<q_x$. The Kramers-Kronig relationship is used to calculate the real part of the correlation function. The $(1,0)q$ or $(0,1)q$ direction can be handled by the expression,

$$\chi''_{10q}(\omega)=\frac{1}{2\pi}\frac{p_f(p_1)\Theta(p_{f,max}^2-p_1^2)-p_f(p_2)\Theta(p_{f,max}^2-p_2^2)}{\sqrt{(4t\sin q/2)^2-\omega^2}}\Theta\left[1-\left(\frac{\omega}{4t\sin q/2}\right)^2\right], \tag{6}$$

where $p_f(p)=\cos^{-1}[-\mu/2t-\cos(p)]$, $p_{f,max}=\cos^{-1}[-1-\mu/2t]$, $p_1=\sin^{-1}[\omega/4t\sin(q/2)]-q/2$ and $p_2=\sin^{-1}[\omega/4t\sin(q/2)]+q/2$. Unlike the parabolic band structure the anisotropy of the system in the tight-binding band structure restricts the solution of the delta function to different areas of the Fermi surface as the chemical potential approaches to half-filling and for $\vec{q}$ in the $(1,1)q$ direction. For a given ω, the solutions of the delta function come from two different regions of Fermi surface. Only one of these contribute for the $\vec{q}=(1,0)q$ direction, whereas both of them survive in $\vec{q}=(1,1)q$ direction in the long wavelength limit.

First we discuss the results of the second-order calculation in the next section, which shows the FL energy dependencies as a function of band structure and we investigate the repeated scattering case and the Stoner instability. At half-filling with $q=2p_f$, the correlation function diverges in both the real and imaginary part that reflects the SDW instability[34,35] for arbitrary U. We choose $U=t$ throughout the calculation and consider values of $\mu\leqslant -0.1t$. With these parameters there are no instabilities in $\chi(\vec{q},\omega)$, which is discussed later in the section ''Instabilities'' in detail with phase diagram. Except in $\mu\rightarrow 0$ limit, there is no nesting phenomena from short wavelengths that solely contribute to the cutoff energy ξ_0 without affecting the logarithmic behavior. The only sign of the nesting character of the Fermi surface is from long wavelengths. We consider two different regions of μ separately as in anisotropic 2D FL and quasi-1D FL.

A. Second-order calculation of $\Sigma(\vec{p},\xi_{\vec{p}})$

The self-energy at zero temperature for the second-order calculation is given by

$$\Sigma(\vec{p},E>0)=\sum_{\vec{q}} \Theta(E-\xi_{\vec{p}-\vec{q}})\Theta(\xi_{\vec{p}-\vec{q}})U^2\chi(\vec{q},E-\xi_{\vec{p}-\vec{q}}), \tag{7}$$

where $\chi(\vec{q},\omega)$ is the density-density correlation function or the response function. The $\xi_{\vec{p}}^2\ln\xi_{\vec{p}}$ behavior in the imaginary part of the self-energy comes from the linear energy dependence in $\chi''(\vec{q},\omega)$. In the self-energy calculation the energy dependence is mainly determined by the frequency dependence of the density-density correlation function rather than the step functions in the expression for the self-energy. The second-order contribution is common to both the ph and the pp channels and reveals the functional dependence of the FL behavior as a function of chemical potential that we break into two regimes, 2D and quasi-1D.

1. Anisotropic 2D Fermi liquid: $-4t\leqslant\mu\leqslant -t$

As the chemical potential μ goes to zero, flatness of the Fermi surface along the $(1,1)p$ direction develops as can be seen in Fig. 1. Although the Fermi surface develops flat, quasi-one dimensional, regions for $\mu\sim -t$, no signature of quasi-one dimensional behavior is seen in $\Sigma(\vec{p},E)$. Figure 2 shows the evolution of the response function as a function of

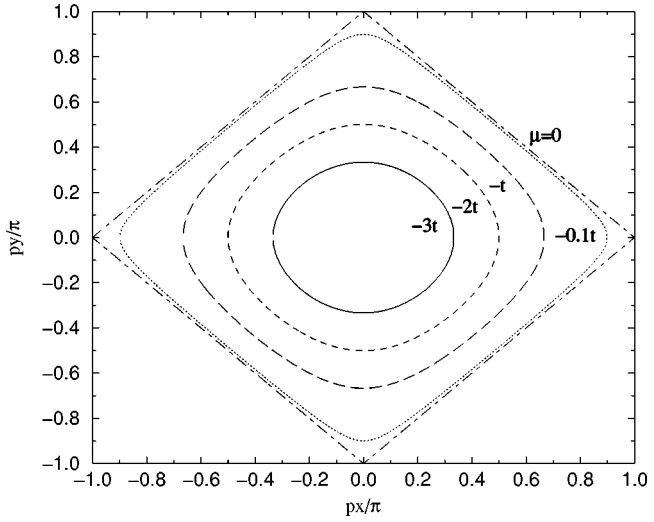

FIG. 1. The band structures for the tight-binding dispersion $\xi_{\vec{p}} = -2t\cos p_x - 2t\cos p_y - \mu$ with different values of μ. As band is filled up, the parabolic Fermi surface is changed to a square surface. For $\mu = -0.1t$, there is a large region of flat Fermi surface.

μ in the directions of $(1,0)q$, $(1,2)q$, and $(1,1)q$ with $q = 10^{-2}\pi$. The cutoff energies, ω_1^* and ω_2^*, come from the two different Fermi surface regions through the delta function for a given momentum $\vec{q}$. Those contributions give two different locations of the divergent peaks ω_1^* and ω_2^*. As $\vec{q}$ points in the (1,1) direction, ω_1^* approaches zero frequency so that the FL linear behavior is limited to small energies. However even in the $(1,1)q$ direction, the linear piece survives and $\Sigma(\vec{p},E)$ has FL behavior for $\mu = -t$. As ω_1^* goes to zero energy, the linear behavior in $\chi''(\vec{q},\omega)$ is limited to a small ω region above which $\chi''(\vec{q},\omega)$ is independent of ω as $\mu \to 0$ as in the one-dimensional system. This will be discussed later. Figure 2 shows the anisotropic band-structure effects, ω_1^* and ω_2^* feature, in the particle-hole correlation function that first appear around $\mu = 2.5t$. Except for the $\mu \sim 0$ case, the $\chi''(\vec{q},\omega)$ follows $\omega/|\vec{q}|$ at small ω that leads to $\xi_{\vec{p}}^2 \ln \xi_{\vec{p}}$ form for $\Sigma''(\vec{p},\xi_{\vec{p}})$.

The log behavior of the imaginary part of the on-shell self-energy, shown in Fig. 3, comes from long wavelengths.

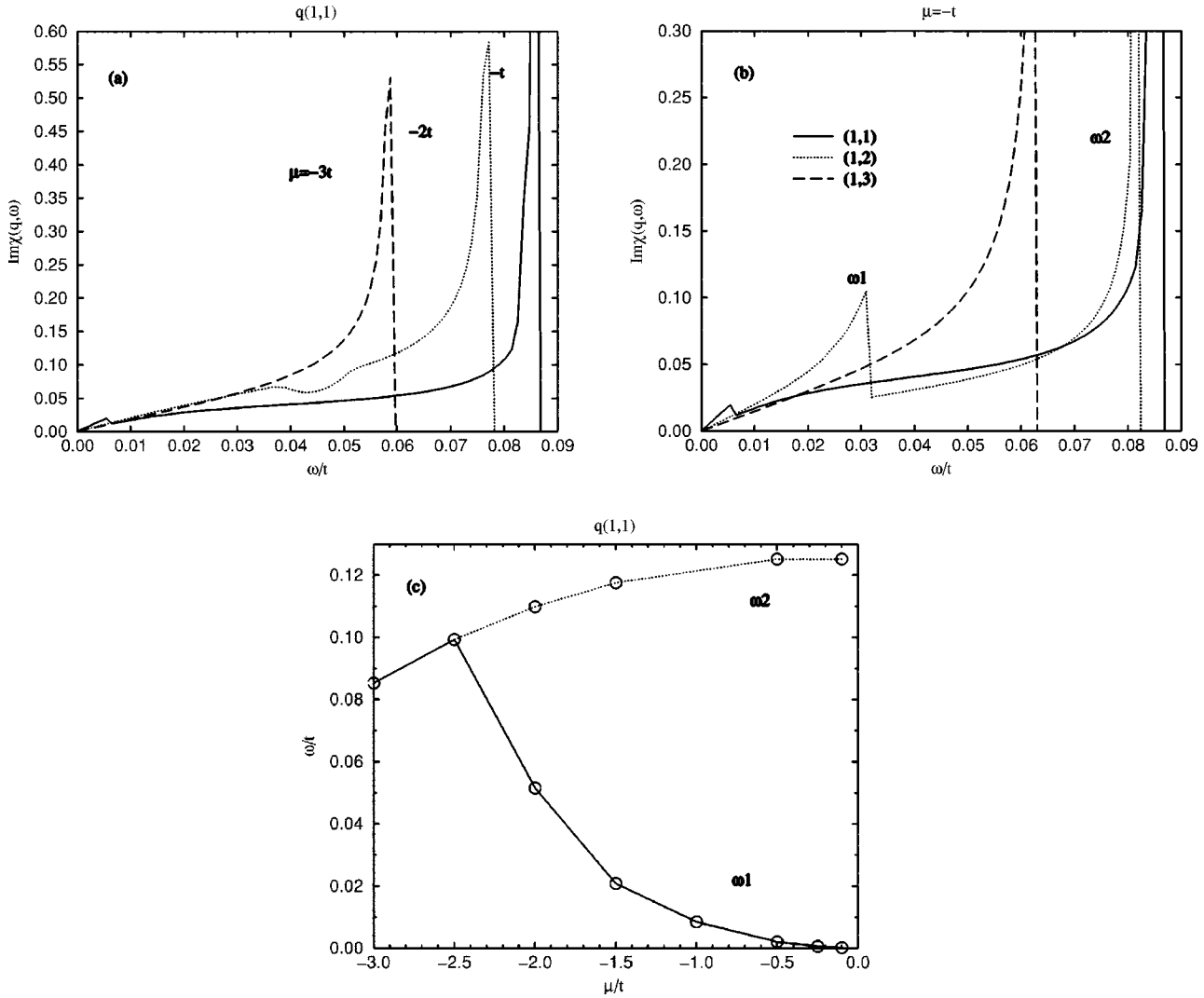

FIG. 2. The correlation functions as a function of μ and directions for $|\vec{q}| = 0.01\pi$. (a) χ'' as a function of μ. Two peaks appeared in χ'' for the anisotropic band structure. (b) χ'' as a function of directions in $\vec{q}$. As $\vec{q}$ points $(1,0)\vec{q}$, ω_1 gets close to ω_2. (c) The locations of peaks in the correlation function, ω_1 and ω_2. As $\mu \to 0$ the location of the first peak approaches to zero.

For small values of $|\xi_{\vec{p}}/t|$, the contributions from longer wavelengths provide the $\xi_{\vec{p}}^2 \ln \xi_{\vec{p}}$ dependencies whereas shorter wavelengths lead to contributions to the $\xi_{\vec{p}}^2$ dependence. The log behavior is restricted by small energy and the long wavelength $|\vec{q}|$'s. The anisotropic 2D systems with $-4t \leqslant \mu \leqslant -t$ shows the generic FL behavior with increasing anisotropy in $\vec{p}$. The correction term is enhanced by tuning the chemical potential close to zero and will be discussed in the next section. The cutoff ξ_0 and β for the two directions of $\vec{p}$ reflect the growing anisotropy of the Fermi surface as μ changes from $-3t$ to $-t$.

2. Quasi-1D behavior: $-t \leqslant \mu \leqslant 0$

The purely one-dimensional response function with a tight-binding band structure $\xi_p = -2t \cos p - \mu$ is

$$\chi''_{1D}(q,\omega) = \frac{1}{2} \frac{\Theta\left(p_f - \left|\frac{q}{2} - \sin^{-1}(\omega/4t \sin q/2)\right|\right) - \Theta\left(p_f - \left|\frac{q}{2} + \sin^{-1}(\omega/4t \sin q/2)\right|\right)}{|4t \sin(q/2)\sqrt{1-(\omega/4t \sin q/2)^2}|} \Theta\left(1 - \left|\frac{\omega}{4t \sin q/2}\right|^2\right), \tag{8}$$

where $p_f = \cos^{-1}(-\mu/2t)$ is the Fermi level for the one-dimensional system. In the small frequency limit there is no energy dependence in χ''_{1D}, which has the corresponding logarithmic divergence in χ'_{1D},

$$\chi'_{1D}(q,\omega=0) = \frac{1}{-4t\,\pi \sin(q/2)} \ln \left|\frac{\tan(p_f - q/2)}{\tan(p_f + q/2)}\right|. \tag{9}$$

In the static limit this divergence at $q = 2p_f$, the so-called perfect nesting vector, drives the Peierls instability via the Kohn anomaly, which leads to the metal-insulator transition.[36]

Coming back to the 2D problem, at $\mu = 0$ the system is one dimensional in that there is perfect nesting between parts on the Fermi surface along the $(1,1)\vec{p}$ direction. Nesting vector, $\vec{q} = (1,1)\pi$, gives a form

$$\chi''(\pi,\pi,\omega;\mu=0) = \frac{\pi}{2} \mathrm{sgn}(\omega) N(\omega/2), \tag{10}$$

where $N(\omega)$ is the density-of-state that has logarithmic divergence at $\omega = 0$. For $\mu = 0$ the constant energy dependence at long wavelengths in $\chi''(\vec{q},\omega)$, which is an one-dimensional effect, lasts up to zero energy (Fig. 4). Using the Kramers-Kronig relationship this energy dependence for small $|\vec{q}|$ in $\chi''(\vec{q},\omega)$ leads to a $\ln \omega$ divergences in the real part $\chi'(\vec{q},\omega)$, signaling the breakdown of random-phase-approximation (RPA). The large $|\vec{q}|$ behavior is shown in Fig. 5 where it is clear that the $\ln \omega$ divergence in $\chi''(\vec{q},\omega)$ is rapidly destroyed as μ goes away from half-filling.

For the $|\vec{q}| < 10^{-1}\pi$ structure of χ'', two divergent peaks identified by ω_1^* and ω_2^*, follows the discussion in the previous section. Due to rapid development of frequency independence in χ'' for low energies as $\mu \to 0$, the quasi-1D corrections to the $\xi_{\vec{p}}^2 \ln \xi_{\vec{p}}$ behavior of $\Sigma''(\vec{p},\xi_{\vec{p}})$ at intermediate values of ω have a $\xi_{\vec{p}}^{3/2}$ dependence in the quasi-particle lifetime. This is shown in Fig. 6 for $\mu = -0.1t$ in which the Fermi surface is flat over an extended area. The $\xi_{\vec{p}}^{3/2}$ correction sets in at $\xi_{\vec{p}} \sim 0.02t$, which limits the generic FL behavior to a small region. The second-order calculation shows that the quasi-particle lifetime has the generic FL dependence with $\mu \neq 0$ with a $\xi_{\vec{p}}^{3/2}$ term as a correction to $\xi_{\vec{p}}^2 \ln \xi_{\vec{p}}$ when $\mu \lesssim 0$.

B. RPA calculation of $\Sigma(\vec{p},\xi_{\vec{p}})$

1. Long-wavelength contribution

With $\mu \neq 0$ the long-wavelength limit contribution, which is responsible for $\xi_{\vec{p}}^2 \ln \xi_{\vec{p}}$ or $\xi_{\vec{p}}^{3/2}$ for $\mu \sim 0$, is renormalized in RPA giving qualitatively the same dependencies. The effective interaction in Eq. (2) for the repeated scattering involves two independent channels, the symmetric and the antisymmetric channels, and is given by

$$U_{eff}(\vec{q},\omega) = \frac{1}{2} \frac{U_s^2 \chi(\vec{q},\omega)}{1 - U_s \chi(\vec{q},\omega)} + \frac{3}{2} \frac{U_a^2 \chi(\vec{q},\omega)}{1 - U_a \chi(\vec{q},\omega)}, \tag{11}$$

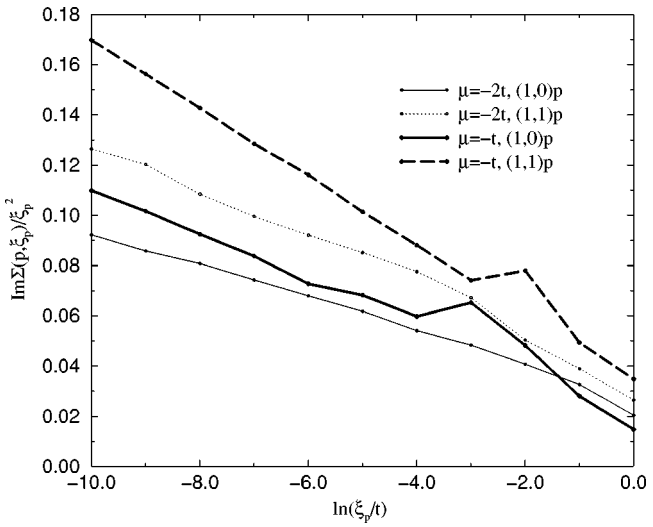

FIG. 3. The imaginary part of self-energies in second-order calculations for $(1,0)p$ and $(1,1)p$ directions with $\mu = -2t$ (thin lines) and $\mu = -t$ (thick lines). Anisotropy increases in the magnitude of the self-energy as μ increases.

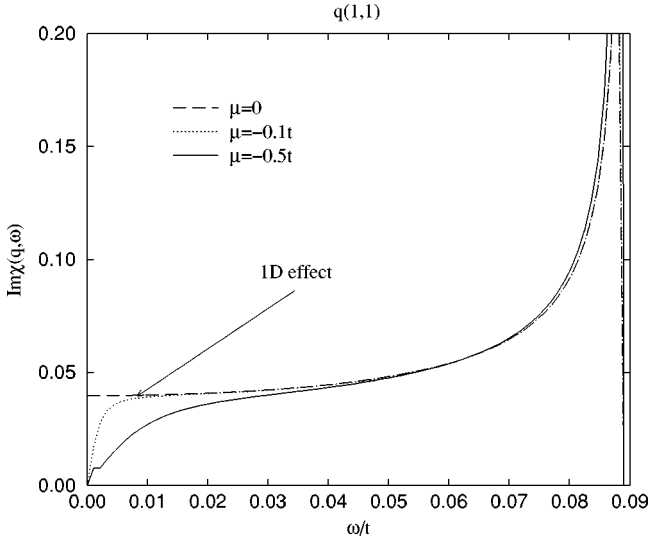

FIG. 4. The correlation functions for $q=0.01\pi$ with different μs. As $\mu\rightarrow 0$, ω independent behavior in low frequency is developed, which is characteristic of 1D feature at long wavelengths and the system shows a 1D effect.

where $U_s=U$ and $U_a=-U$. In RPA, the imaginary part of the self-energy $\Sigma''(\vec{p},\xi_{\vec{p}})$ is just enhanced from the second-order calculations as in Fig. 7. The $\mu=-0.1t$ case includes $\xi_{\vec{p}}^{3/2}$ corrections in the $(1,0)p$ direction. The real part $\Sigma'(\vec{p},\xi_{\vec{p}})$ has the $\xi_{\vec{p}}|\xi_{\vec{p}}|$ correction to the $\xi_{\vec{p}}$ term, which comes from the long wavelength and is shown in Fig. 8. The $\xi_{\vec{p}}|\xi_{\vec{p}}|$ term is a mirror of $\xi_{\vec{p}}^2\ln\xi_{\vec{p}}$ term in $\Sigma''(\vec{p},\xi_{\vec{p}})$ through the Kramers-Kronig relationship and the deviations from the fits are consistent with both the $\Sigma''(\vec{p},\xi_{\vec{p}})$ and $\Sigma'(\vec{p},\xi_{\vec{p}})$ graphs. The on-shell calculation of the $\xi_{\vec{p}}|\xi_{\vec{p}}|$ term in the (1,0) direction with $\mu=-0.1t$ stops at $\xi_{\vec{p}}\sim 0.05t$ because the phase space runs out for that direction and the correction to the $\xi_{\vec{p}}|\xi_{\vec{p}}|$ term sets in earlier than the (1,1) direction. The coefficients of the $\xi_{\vec{p}}|\xi_{\vec{p}}|$ terms for the two directions are different due to the anisotropy of the system.

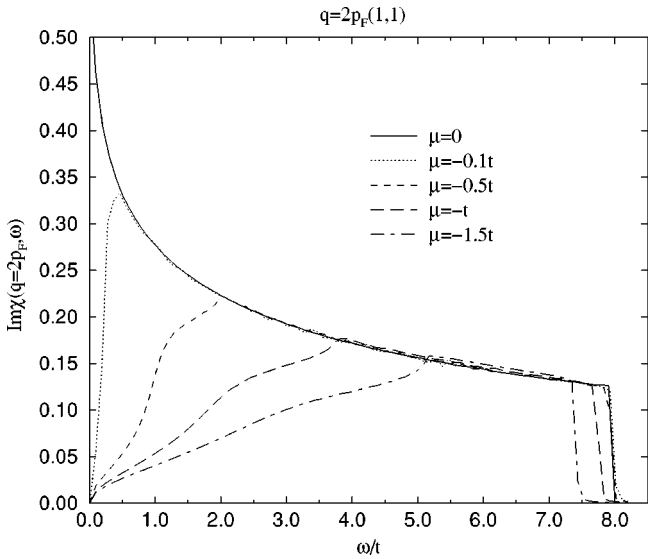

FIG. 5. The correlation functions for $q=2p_F$ with different μs. As $\mu\rightarrow 0$ logarithmic divergence is rapidly developed near $\mu\sim 0$.

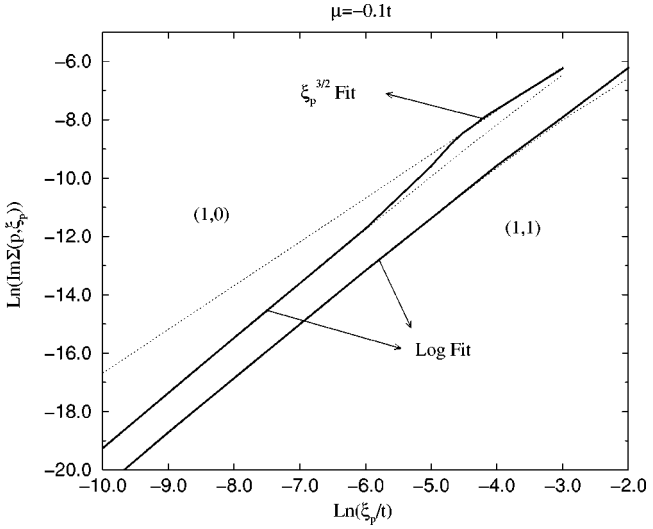

FIG. 6. The imaginary part of self-energy in second-order calculations with $U=t$ shows $\xi^{3/2}$ behavior, which is coming from frequency independent χ''. This crossover from $\xi_{\vec{p}}^2\ln\xi_{\vec{p}}$ to $\xi_{\vec{p}}^{3/2}$ appears in the $(1,0)p$ direction. The dotted lines are fitted lines.

Figure 9 shows the functional dependence of the cut-off energy in the imaginary part of the self-energy $\xi_{0,\vec{p}}$ and the coefficients $\beta_{\vec{p}}$ for the tight-binding band structure. The anisotropy from $\beta_{\vec{p}}$ grows as the band is filled, but near half-filling the trend changes rapidly due to the flatness of the band structure. The cutoff energy shows anisotropy even at $\mu=-3t$, which is different from Fig. 2 in which the anisotropic effects of splitting the two different peaks in $\chi''(\vec{q},\omega)$ are shown.

2. Instabilities

As discussed above the correlation function itself does not indicate any instability unless $\mu=0$ as in Fig. 4. For the

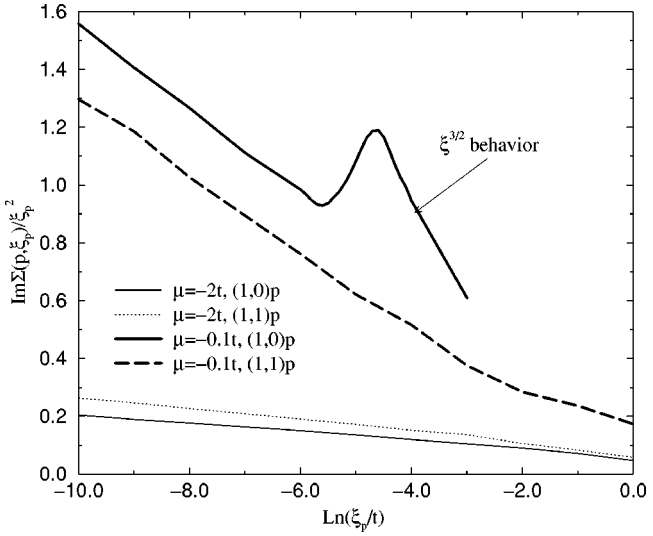

FIG. 7. The imaginary part of self-energies in RPA with $U=t$ for $(1,0)p$ and the $(1,1)p$ directions with $\mu=-2t$ (thin lines) and $\mu=-0.1t$ (thick lines). For the $\mu=-0.1t$ case, $\xi_{\vec{p}}^{3/2}$ behavior for the $(1,0)p$ direction appears as in the second-order calculation. Both of the directions show the logarithmic behavior.

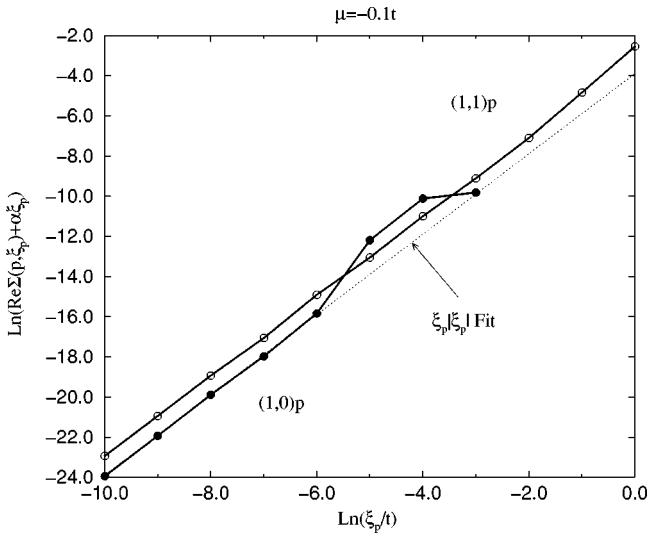

FIG. 8. The real part of self-energy calculated in RPA with $U=t$ shows $\xi|\xi_{\vec{p}}|$ behavior correction to the $\alpha\xi_{\vec{p}}$ term. The slope 2 indicates the power of the fit. The deviation from the $\xi_{\vec{p}}|\xi_{\vec{p}}|$ behavior comes from the long-wavelength quasi-1D frequency dependence of $\chi(\vec{q},\omega)$.

repulsive interaction the effective interaction in the antisymmetric channel could have an instability indicated by a pole at $\omega=0$. The solution for it is given by $1/U_c=\chi'(\vec{q},\omega=0)$ in RPA so that there are solutions for all U's. Within the RPA the question is how fast the system goes to 1D as a band approaches to half-filling.

In a parabolic band structure, the real part of the correlation function in the static limit is given by

$$\chi_{1D}(q)=N_{1D}(0)\frac{1}{2(q/2p_f)}\ln\left|\frac{1+(q/2p_f)}{1-(q/2p_f)}\right|, \quad (12a)$$

$$\chi_{2D}(q)=N_{2D}(0)\left[1-\sqrt{\frac{(q/2p_f)^2-1}{(q/2p_f)}}\Theta\{(q/2p_f)-1\}\right], \quad (12b)$$

$$\chi_{3D}(q)=N_{3D}(0)\left[\frac{1}{2}+\frac{1-(q/2p_f)^2}{4(q/2p_f)}\ln\left|\frac{1+(q/2p_f)}{1-(q/2p_f)}\right|\right], \quad (12c)$$

where the $N(0)$'s are the densities-of-state on the Fermi level for each dimension and Θ is a step function. In 2D the correlation function has a cusp and a discontinuous derivative at $q=2p_f$ due to the step function, whereas the 3D case varies smoothly. Since the Fermi surface consists of two points in 1D, the nesting condition $\xi_{\vec{p}}-\xi_{2\vec{p}_f-\vec{p}}=0$ is satisfied over the entire Fermi surface resulting in a log divergence at $q=2p_f$. This is responsible for the breakdown of the FL ground state leading to a metal-insulator transition.

In Fig. 10 the static correlation function in the $(1,1)\vec{q}$ direction has a developing divergence at $|\vec{q}|=2p_f^{(1,1)}$ as the system changes from 2D to 1D. The function is repeated at $|\vec{q}|=\pi$ due to periodic lattice where $|\vec{q}|=\pi$ is at the middle

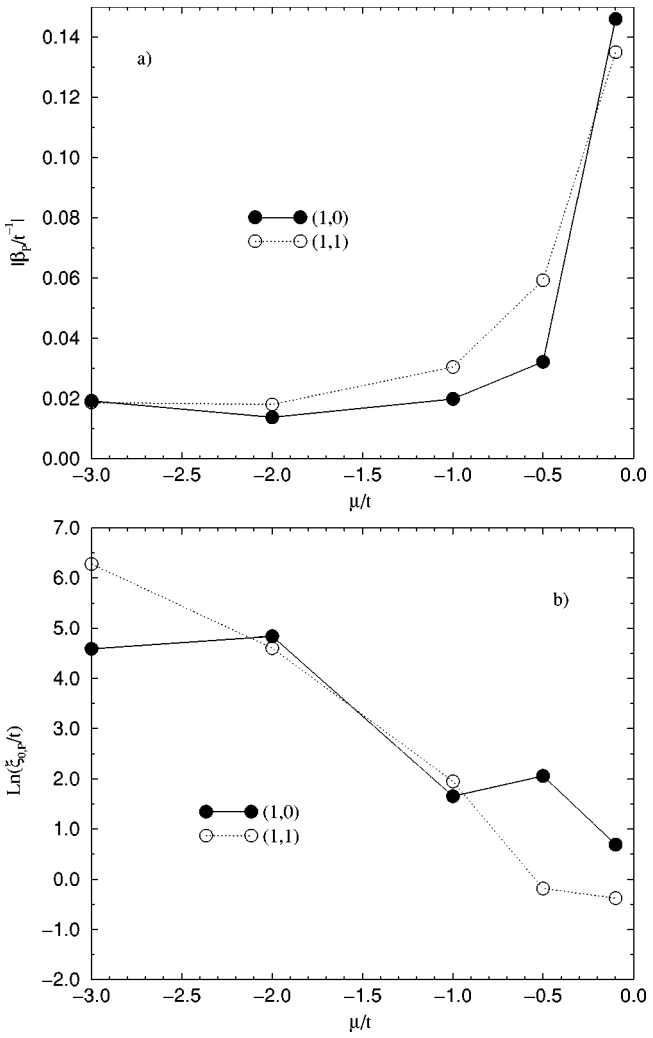

FIG. 9. The slopes $\beta_{\vec{p}}$ (b) and the cutoff energies $\xi_{0,\vec{p}}$ (a) in RPA as a function of μ from the form $\Sigma''(\vec{p},\xi_{\vec{p}})=-\beta_{\vec{p}}\xi_{\vec{p}}^2\ln[\xi_{\vec{p}}/\xi_{0,\vec{p}}]$.

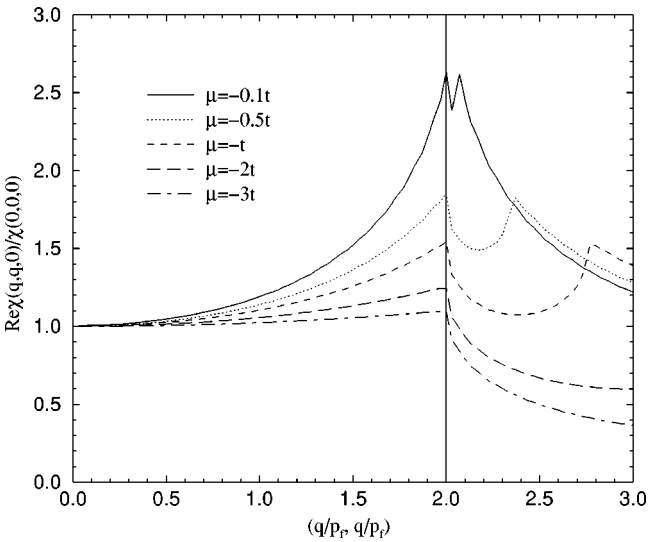

FIG. 10. The real part of the correlation function in static limit. The system changes 2D to 1D as $\mu\to0$. A divergence grows at $q=2p_f$ as $\mu\to0$ in the $(1,1)q$ direction.

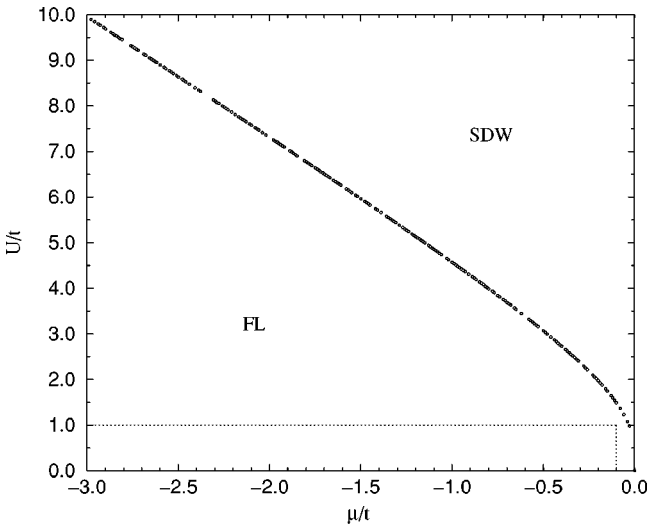

FIG. 11. The phase diagram of the system from $1-U_c\chi'(2p_f,2p_f,0)=0$. For any strength of interaction at $\mu=0$ the FL ground state breaks down due to the divergence. With $U=t$, there is no SDW instability for $\mu<-0.1t$.

of the dip, right next to the peak. The $\mu=-3t$, which has the Fermi surface close to circle, shows constant q dependence with densities-of-state

$$N(\mu)=\lim_{\vec{q}\to 0}\lim_{\omega\to 0}\chi'(\vec{q},\omega) \tag{13}$$

as in the parabolic band case. The phase diagram U vs μ is calculated by $1/U=\chi'(2p_f,2p_f,\omega=0)$. With an interaction strength of $U=t$, the Stoner instability does not occur until $\mu\sim-0.03t$. In the calculations discussed in this paper $U=t$ (dotted line in Fig. 11) so that the instability of the system is absent except when $\mu\sim 0$ for $U\leqslant t$.

This conclusion is supported by a recent renormalization-group analysis of the Hubbard model by Halboth and Metzner[37] who found that the tendency towards the antiferromagnetic nesting instability is limited to $\mu\gtrsim-0.1t$ for $U=t$ as evidenced by a growing spin susceptibility. They found in fact that $d_{x^2-y^2}$ superconductivity fluctuations provide the dominant susceptibility further from half-filling but even these were suppressed beyond $\mu\sim-0.01t$. The influence of superconducting fluctuations are missing in the present calculation.[38]

Going beyond this weak-coupling region is difficult because of the uncontrolled nature of the RPA. One such attempt is the so-called self-consistent fluctuation exchange approximation (FLEX) which however is equally uncontrolled. It has been pointed out by Vilk and Tremblay[39] that the absence of vertex corrections in the FLEX leads to even more severe breakdowns of sum rules than does the RPA discussed here. Vilk and Tremblay have proposed an improvement in RPA to ensure that the sum rules are satisfied. In their approach the influence of the cross channels in the ph expansion on the vertices is mimicked by letting the irreducible vertices in the charge and spin channels be independent of each and chosen to satisfy sum rules. In this approach SDW fluctuations above $T=0$ lead to the breakdown of the quasiparticle approximation for $U=4t$. These approaches have been limited to finite size systems and so miss

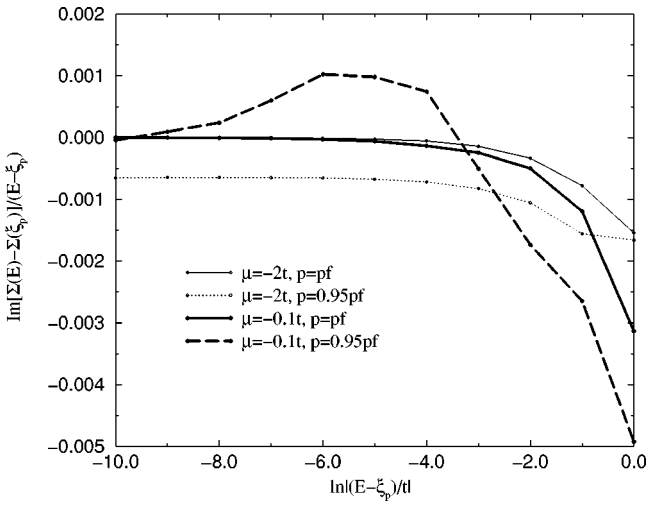

FIG. 12. The imaginary part of the off-shell self-energy for $E<0$ and $p<p_f$ in second-order calculations. $E\to\xi_p^-$ limit $\Sigma''(\vec{p},E)$ has constant energy term $\xi_p^2\ln\xi_p^-$ for $\mu=-2t$ in the $ln|E-\xi_p^-|$ scale in the case of $p\neq p_f$. There is a significant deviation in $\Sigma''(\vec{p},E)$ for $\mu=-0.1t$ in the case of $p\neq p_f$.

the long-wavelength interactions responsible for the leading corrections of interest in the present paper.

C. Off-shell calculations, $\Sigma(\vec{p},E)$: Spectral function

The spectral function can be measured by ARPES and is given by

$$A(\vec{p},E)=\frac{|\Sigma''(\vec{p},E)|}{[E-\xi_p^--\Sigma'(\vec{p},E)]^2+[\Sigma''(\vec{p},E)]^2}, \tag{14}$$

where the off-shell self-energies are involved. For large cutoff momentum q_c, and the parabolic band structure, the leading contributions to the imaginary part of off-shell self-energy that determines the width of the spectral function has a form[24]

$$\Sigma''(\vec{p},E)=C[\{\xi_p^2+2\xi_p^-(E-\xi_p^-)\}\ln(\max[\xi_p^-,|E|])+(E-\xi_p^-)^2\ln(|E-\xi_p^-|)], \tag{15}$$

where C is a constant. In Fig. 12 $[\Sigma''(\vec{p},E)-\Sigma''(\xi_{p,\vec{p}}^-)]/(E-\xi_p^-)$ vs $\ln|E-\xi_p^-|$ is plotted for $E-\xi_p^-<0$. In the limit $(E-\xi_p^-)\to 0$ we find $2C\xi_p^-\ln|\xi_p^-|$ consistent with Eq. (15) for a given $\vec{p}$. For $\mu=-2t$ the Fermi surface is close to parabolic band structure and the off-shell self-energy has a $(E-\xi_p^-)$ independent behavior for small values of $(E-\xi_p^-)$ as in the Eq. (15). For $\mu=-0.1t$ the $\Sigma''(p_f,E)$ is consistent with Eq. (15). However for $p=0.95p_f$, although $\Sigma''(\vec{p},\xi_p^-)$ still has the $\xi_p^2\ln\xi_p^-$ dependence, $\Sigma''(\vec{p},E)$ is seen to deviate from the form given in Eq. (15). The dependence on E in Fig. 13 shows a $E^2\ln|E|$ behavior for $\mu=-2t$ only for $p=p_f$ and the more complicated dependence shown in Eq. (15) is found for $|\vec{p}|\neq p_f$. This is the case for other values of μ also. This indicates that the form $E^2\ln E$ for $\Sigma(\vec{p},E)$ frequently used in the literature is a poor approximation[40,41] to the more complicated function of $\vec{p}$ and E.

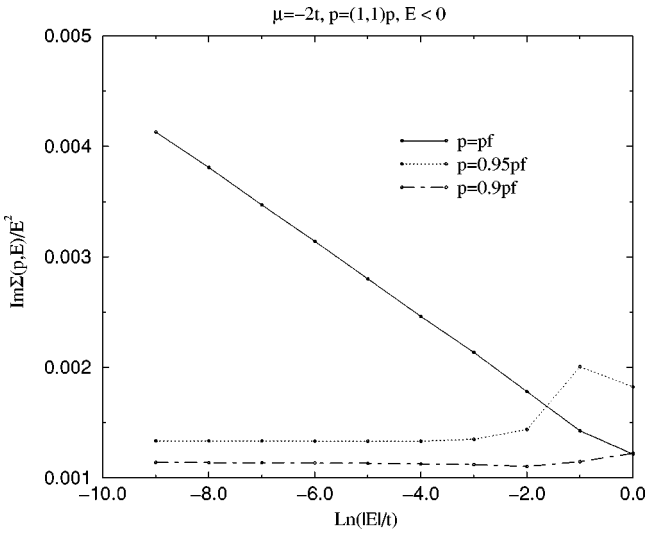

FIG. 13. The graph shows that the off-shell self-energy follows $E^2 \ln E$ only when $p = p_f$ even for $\mu = -2t$, which is close to parabolic band structure.

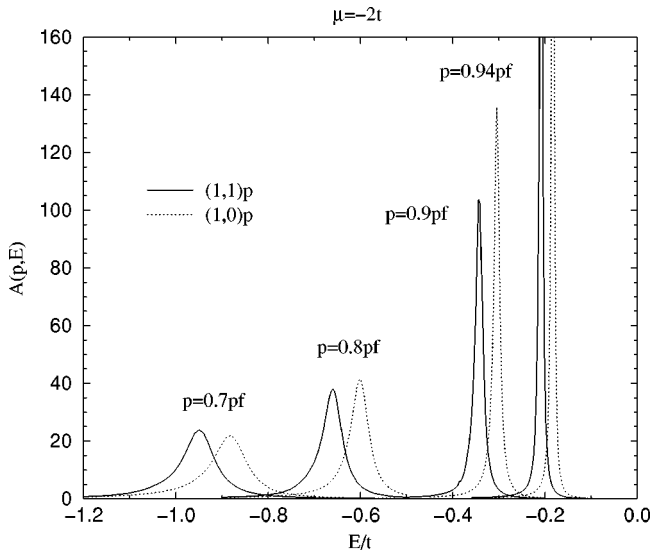

FIG. 14. The spectral functions in repeated scattering calculations for $\mu = -2t$ in $(1,1)\vec{p}$ (solid lines) and $(1,0)\vec{p}$ (dotted lines) directions. The quasiparticle peaks are well defined as $p \to p_f$. Asymmetry in the resonance peak appears when $p \sim p_f$.

ARPES data is analyzed in terms of the single-particle spectral density. The extent to which a quasiparticle resonance is well defined is characterized by the width of the resonance at half-maximum. This is frequently thought of as a measure of the quasiparticle lifetime where the momentum dependence is taken as a test of the Fermi-liquid character of the material under investigation. When the quasiparticle approximation is applied, the spectral function is

$$A(\vec{p},E) = \frac{\Gamma_{\vec{p}}}{(E - E_{\vec{p}})^2 + \Gamma_{\vec{p}}^2}, \tag{16}$$

where $E_{\vec{p}}$ is the location of the resonance and $\Gamma_{\vec{p}}$ is half-maximum width of the peak. Here we apply this analysis to the Hubbard model.

The spectral functions are calculated for the $\mu = -2t$ and $\mu = -0.1t$ cases and the widths of the resonance at the half of the peak $\Gamma_{\vec{p}}$ are plotted as a function of $\xi_{\vec{p}} < 0$. The spectral functions are picked along Γ to Y point and to $\bar{M}$ point. The quasiparticle peaks are well defined and as $p \to p_f$, the resonance gets sharper for the $(1,0)p$ and $(1,1)p$ directions in Fig. 14 for $\mu = -2t$. The $\mu = -0.1t$ case in Fig. 15 has the same feature except for a growing anisotropic feature for the $(1,1)p$ direction deep inside the Fermi surface. There is no sign of the pseudogap with the parameters used in this calculations for $\mu = -2t$ and $\mu = -0.1t$. As $p \to p_f$ the resonance peak does not show symmetry about $E = E_{\vec{p}}$ since the imaginary part of the self-energy is always zero for $E = 0$. $A(\vec{p},E)$ is only symmetric about $E = 0$ for $|\vec{p}| = |p_f|$. The smallest deviation from p_f leads to strongly nonsymmetric $A(\vec{p},E)$. This indicates that one can be misled by assuming symmetry for the ARPES data cutoff by Fermi Dirac distribution function[42] to get the single-particle properties near Fermi surface.

If we expand $A(\vec{p},E)$ near $E_{\vec{p}} = \xi_{\vec{p}} + \Sigma'(\vec{p},E)$, which is approximately the location of the resonance peak since $\Sigma(\vec{p},E)$ is continuous, the width of half maximum is given by the on-shell self-energy

$$\Gamma_{\vec{p}} \sim \frac{z_{\vec{p}} \Sigma''(\vec{p},E_{\vec{p}})}{\sqrt{1 + [z_{\vec{p}} \partial \Sigma''(\vec{p},E)/\partial E|_{E=E_{\vec{p}}}]^2}}, \tag{17}$$

where $z_{\vec{p}} = [1 - \partial \Sigma'(\vec{p},E)/\partial E|_{E=E_{\vec{p}}}]^{-1}$ unless $\Sigma''(\vec{p},E)$ has strong energy dependencies. In this calculation we find $1 - z_{\vec{p}} \lesssim 3\%$ showing that there is very little frequency dependence in the real part $\Sigma'(\vec{p},E) \sim \Sigma'(\vec{p},\xi_{\vec{p}})$. Figure 16 shows the agreement between the half maximum width and the on-shell self-energy at low energies $\Gamma_{\vec{p}} \sim \Sigma''(\vec{p},\xi_{\vec{p}})$ for $\mu = -2t$ and $\mu = -0.1t$. As in the figure the generic FL logarithmic behavior is restricted to low energies. For the $\mu = -2t$ case $\Gamma_{\vec{p}}$ shows linear behavior in $\xi_{\vec{p}}$ at higher energies which are not extrapolated to zero energy. Clearly the assumption that a deviation from $\Gamma_{\vec{p}} \sim \xi_{\vec{p}}^2 \ln \xi_{\vec{p}}$ or $\xi_{\vec{p}}^2$ is an indication of non-Fermi liquid is not correct. We note that no sign of the complicated $\xi_{\vec{p}}$ and E dependencies of $\Sigma(\vec{p},E)$, shown in Eq. (15), comes out of this analysis of ARPES data. It seems to us unlikely that it will be possible to recover these dependencies without prior knowledge of the functional form with which to fit the data.

III. CONTRIBUTIONS FROM THE PARTICLE-PARTICLE CHANNEL

Fukuyama *et al.*[43] have investigated the contribution to $\Sigma''(\vec{p},E)$ for the pp channel using the parabolic dispersion. The contribution to $\Sigma(\vec{p},E)$ in second order in the interaction can be thought of as being in either the ph or pp channel. In the second-order calculation the difference between the two channels is that the $\xi_{\vec{p}}^2 \ln \xi_{\vec{p}}$ contribution comes from propagating particle or hole pairs with momenta $q \sim 2p_f$ in the pp channel whereas it comes from long-wavelength particle-hole pairs in the ph channel. Taking the second-order diagram to be in the pp channel contribution, its con-

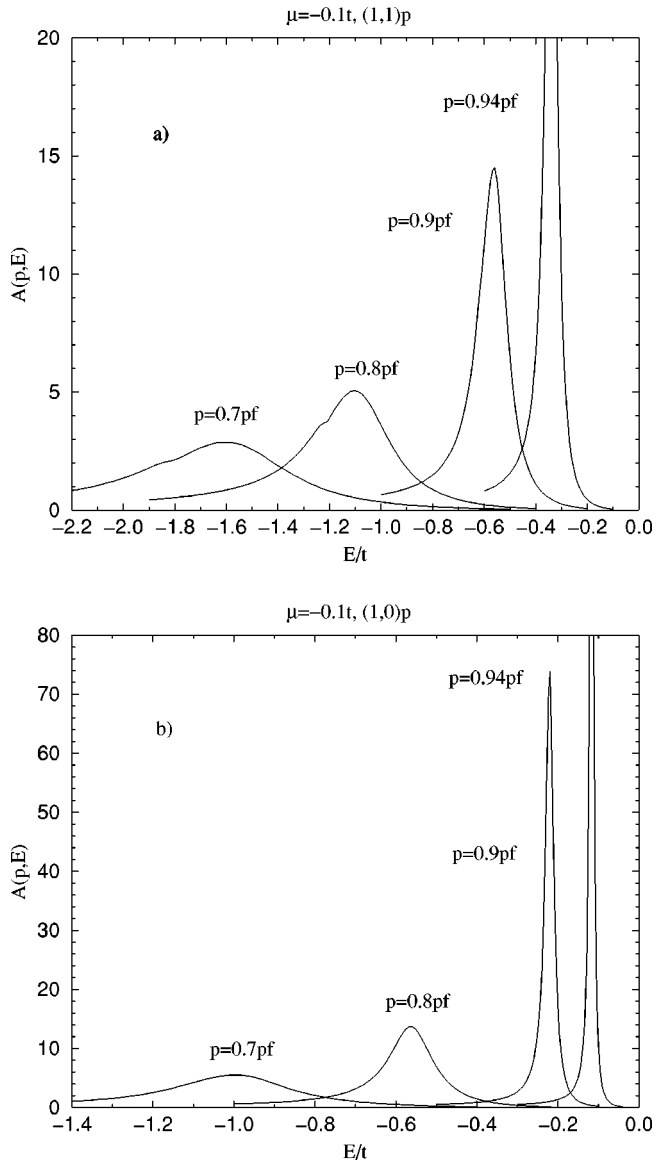

FIG. 15. The spectral functions in repeated scattering calculations for $\mu=-0.1t$ in the $(1,1)\vec{p}$ (a) and $(1,0)\vec{p}$ (b) directions. The quasiparticle peaks are well defined as $p\rightarrow p_f$. Asymmetry in the resonance peak appears for $(1,1)\vec{p}$ deep inside of the Fermi surface.

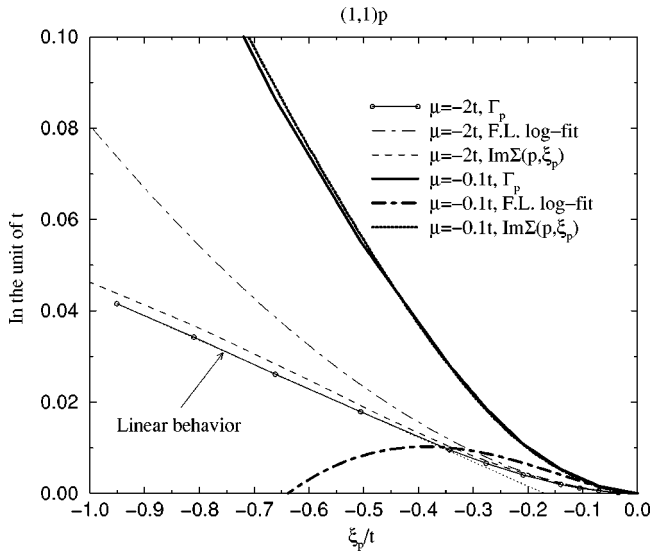

FIG. 16. The comparison between $\Gamma_{\vec{p}}$ and on-shell self-energy for $\mu=-2t$ (thin lines) and $\mu=-0.1t$ (thick lines). The FL behavior $\xi_{\vec{p}}^2\ln\xi_{\vec{p}}$ is restricted to low energies.

tribution is screened by repeated scattering in that channel. In contrast to the case of an attractive interaction there is no Cooper instability but instead the contribution is reduced by the repeated scattering. Unlike the situation in the ph channel the result is not simply an enhancement or reduction of the contribution from the second-order diagram giving $\xi_p^2\ln\xi_p$ contribution to $\Sigma''(p,\xi_p)$ again. Rather there is a strong momentum dependence in the real part of the pp propagator at $q\sim 2p_f$, which eliminates the $\xi_p^2\ln\xi_p$ dependence. As a result the effect of including the pp channel in a calculation of $\Sigma(p,E)$ is to remove the contribution of the second-order term in the interaction from leading dependencies. The pp contribution to $\Sigma(p,E)$ in a tight-binding band structure remains to be worked out in detail. However the result is unlikely to be quantitatively different from the result for the parabolic band. Indeed for particle pairs/hole pairs with net momentum $\vec{Q}=(\pi,\pi)$ it is easy to show that the propagator $K(\vec{Q},\omega)\sim(1/\omega+2\mu)f(\mu)$, where $f(\mu)$ is a polynomial in μ and gives a vanishingly small contribution to $\Sigma(p,E)$, where the consequences of the almost nested Fermi surface would be expected to be greatest.

There have been a number of investigations of collective modes in the pp channel. Engelbrecht and Randeria[44] found a collective mode below the two-particle continuum in a bound state of hole pairs that arises because of the finite density-of-states at bottom of the band in 2D. The contribution of this mode to the self-energy is given by $\Sigma''(p_f,E)\sim\mu|E/E_a|^{5/2}$ where μ is the chemical potential and E_a is an energy scale describing the interaction. So this mode does not contribute to the leading dependencies in $\Sigma''(p,E)$. Yang[45] and more recently Demler and Zhang[46] have found evidence for a different singlet and triplet collective mode in the pp channel that exists in a narrow region of momenta near (π,π). The narrow range of momenta suggests that this mode can have little effect on the low-energy properties of $\Sigma(p,E)$.

In summary neither the continuum nor collective-mode contributions from the pp channel contribute to the leading dependencies in $\Sigma(p,E)$.

IV. CONCLUSION AND SUMMARY

We have demonstrated that, within weak-coupling RPA, the anisotropy in band structure does not qualitatively change the FL dependencies. We have done that by calculating the single-particle properties in the Hubbard model in which the shape of the Fermi surface is changed from a circle to a square as the value of the chemical potential is varied from $\mu=-3t$ to $\mu=-0.1t$. In these calculations we have used a weak-coupling approximation in which the magnitude of the interaction U is far from the values for the SDW instability except for $\mu>-0.5t$. Numerical coefficients in the functional forms of the imaginary part of the self-energy reflect the anisotropy of the band structure but it is not until the Fermi surface is almost a square that the first

sign of the quasi-1D behavior $\xi_{\vec{p}}^{3/2}$ appears. As $\mu \to 0$ the magnitude of $\Sigma''(\vec{p},\xi_{\vec{p}})$ increases with increasing anisotropy. Also, in the $\mu \to 0$ limit, an ω independent region in $\chi''(\vec{q},\omega)$ grows, which is responsible for $\xi_{\vec{p}}^{3/2}$ behavior in $\Sigma''(\vec{p},\xi_{\vec{p}})$ in $(1,0)p$ direction. The $\xi_{\vec{p}}|\xi_{\vec{p}}|$ term is also found in $\Sigma'(\vec{p},\xi_{\vec{p}})$ as in the parabolic band case. The instability of the system is slowly developed as the system goes to 1D except $\mu \sim 0$.

The off-shell self-energy is shown to have a similar $\vec{p}$ and E dependence as in the parabolic band with deviations as the Fermi surface develops flat regions. In this region we confirmed the half maximum width of the resonance peak for spectral function is approximated by the on-shell self-energy. Asymmetry in the resonance peak grows for $|\vec{p}| \to p_f$ due to $\Sigma''(\vec{p},E=0)=0$. This is also the case deep inside the Fermi surface for $\mu=-0.1t$ and the $(1,1)|\vec{p}|$ direction. In the tight-binding band structure, the quasiparticle picture is well defined for $\mu < -0.1t$ and $|U| \lesssim t$.

The results found here for the Hubbard model for the leading dependence of $\Sigma(\vec{p},E)$ are applicable to more general Hamiltonians in which the interaction among the quasiparticles depends on momentum transfer since these leading dependencies in $\Sigma(\vec{p},E)$ are determined by the long-wavelength limit of the quasiparticle interaction rather than its detailed form. The results demonstrate that there is qualitative change in the $\vec{p}$ and E dependence of $\Sigma(\vec{p},E)$ only for very close proximity to nesting features in the band structure.

The single band Hubbard model has been used extensively as a model for the normal state properties of cuprates. Many of these investigations have emphasized proximity to van Hove singularity[28,29,47,48] to explain derivations from FL temperature dependencies and even so-called the marginal FL behavior of $\Sigma(\vec{p},E)$. The approximation used in these papers lead to non-FL behavior. The present results show that no such effects are present in the single band Hubbard model in the RPA and that any treatment that arrives at non-FL behavior using the weak-coupling RPA should be viewed with caution.

Detailed ARPES data is available on the cuprates also which shows the quasiparticle resonance is absent in the underdoped region over an extended range of doping. This is understood in terms of a pseudogap in which weight in the spectral density is shifted to the incoherent background at higher energies. In the RPA treatment considered here the quasiparticle resonances are found to be well defined even at $\mu=-0.1t$, where the Fermi surface is almost perfectly nested and the Stoner factor is $1-U_c\chi(Q,0) \simeq 1/3$. Even for this extreme value of μ no evidence is found for pseudogap behavior. This suggests that the Hubbard model does not describe the low-energy behavior of the cuprates in the RPA.

As one goes further away from the weak-coupling parameter region it becomes difficult to justify the simple RPA weak-coupling approximation used here. SDW and superconducting fluctuations are likely to play a role as other authors have pointed out. Their effects on the leading dependencies from long wavelengths in $\Sigma(\vec{p},E)$ remain to be investigated.

If the single band Hubbard model is to describe the cuprates, one needs to go beyond RPA. Tremblay and coworkers have introduced a variation of the vertices in the singlet and triplet channels with doping on the basis of sum rules. This leads to very strong interaction with damped magnons of magnetically ordered $T=0$ phase when $U=4t$ as $T \to 0$. These calculations are carried out a finite size systems and cannot address the issues discussed here. Even though increasing the magnitude of U in the RPA will give qualitatively the same behavior as $U \to 0$, there are likely to be large quantitative corrections especially as the Stoner criterion for an instability is approached. An alternative to this weak-coupling approach is to investigate the FL behavior of the t-J model and investigate $\Sigma(\vec{p},E)$ due to higher powers of $1/U$ for this model. This remains to be investigated.

[1] D. Pines and P. Nozieres, *The Theory of Quantum Liquids* (Benjamin, New York, 1966), Vol. 1.

[2] J.G. Bednorz and K.A. Müller, Z. Phys. B: Condens. Matter **64**, 189 (1986).

[3] T. Timusk and R. B. Tanner, in *Infrared Properties of High T_c Superconductors*, edited by D. M. Ginsberg (World Scientific, Singapore, 1988), Vol. 1.

[4] H. Takagi, B. Batlogg, H.L. Kao, J. Kwo, R.J. Cava, J.J. Krajewski, and W.F. Peck, Phys. Rev. Lett. **69**, 2975 (1992).

[5] Y. Ando, G.S. Boebinger, A. Passner, T. Kimura, and K. Kishio, Phys. Rev. Lett. **75**, 4662 (1995).

[6] Y. Ando, G.S. Boebinger, A. Passner, N.L. Wang, C. Geibel, and F. Steglich, Phys. Rev. Lett. **77**, 2065 (1996).

[7] M.C. Schabel, C.H. Park, A. Matsuura, Z.X. Shen, D.A. Bonn, X. Liang, and W.N. Hardy, Phys. Rev. B **57**, 6090 (1998); **57**, 6107 (1998).

[8] M.R. Norman, H. Ding, M. Randeria, J.C. Campuzano, T. Yokoya, T. Takeuchi, T. Takahashi, T. Mochiku, K. Kadowaki, P. Guptasarma, and D.G. Hinks, Nature (London) **392**, 157 (1998); J. Mesot, A. Kaminski, H.M. Fretwell, M. Randeria, J.C. Campuzano, H. Ding, M.R. Norman, T. Takeuchi, T. Sato, T. Yokoya, T. Takahashi, I. Chong, T. Terashima, M. Takano, T. Mochiku, and K. Kadowaki, cond-mat/9910430 (unpublished).

[9] P.W. Anderson, Phys. Rev. Lett. **64**, 1839 (1990); **65**, 2306 (1990).

[10] C. Castellani, C. Di Castro, and W. Metzner, Phys. Rev. Lett. **69**, 1703 (1992).

[11] C. Castellani, C. Di Castro, and W. Metzner, Phys. Rev. Lett. **72**, 316 (1994).

[12] D. Boies, C. Bourbonnais, and A.-M.S. Tremblay, Phys. Rev. Lett. **74**, 968 (1995).

[13] P. Kopietz, V. Meden, and K. Schönhammer, Phys. Rev. B **56**, 7232 (1995).

[14] H. Ding, M.R. Norman, T. Yokaya, T. Takeuchi, M. Randeria, J.C. Campuzano, T. Takahashi, T. Mochiku, and K. Kadowaki, Phys. Rev. Lett. **78**, 2628 (1997).

[15] A.G. Loeser, Z.-X. Shen, M.C. Schabel, C. Kim, M. Zhang, A. Kapitulnik, and P. Fournier, Phys. Rev. B **56**, 14 185 (1997).

[16] J. Mesot, A. Kaminski, H.M. Fretwell, M. Randeria, J.C. Campuzano, H. Ding, M.R. Norman, T. Takeuchi, T. Sato, T. Yokoya, T. Takahashi, I. Chong, T. Terashima, M. Takano, T. Mochiku, and K. Kadowaki, cond-mat/9910430 (unpublished).
[17] S.A. Trugman, Phys. Rev. Lett. **65**, 500 (1990).
[18] A. Moreo, D.J. Scalapino, R.L. Sugar, S.R. White, and N.E. Bickers, Phys. Rev. B **41**, 2313 (1990).
[19] R. Eder and Y. Ohta, Phys. Rev. B **51**, 6041 (1995).
[20] E. Dagotto, A. Nazarenko, and M. Boninsegni, Phys. Rev. Lett. **73**, 728 (1994).
[21] J. Kim and D. Coffey, Phys. Rev. B **57**, 542 (1998).
[22] C. Hodges, H. Smith, and J. W. Wilkins, Phys. Rev. B **4**, 302 (1971).
[23] P. Bloom, Phys. Rev. B **12**, 125 (1975).
[24] D. Coffey and K. Bedell, Phys. Rev. Lett. **71**, 1043 (1993).
[25] J. M. Williams, J. R. Ferraro, and R. J. Thorn, *Organic Superconductors (including Fullerenes) : Synthesis, Structure, Properties and Theory* (Prentice Hall, Englewood Cliffs, 1992).
[26] J. Kim and D. Coffey (unpublished).
[27] J. Kim and D. Coffey, Philos. Mag. B **74**, 477 (1996).
[28] A. Virosztek and J. Ruvalds, Phys. Rev. B **42**, 4064 (1990).
[29] J. Ruvalds and A. Virosztek, Phys. Rev. B **43**, 5498 (1991).
[30] R. Hlubina and T.M. Rice, Phys. Rev. B **51**, 9253 (1995).
[31] L.B. Ioffe and A.J. Millis, Phys. Rev. B **58**, 11 631 (1998).
[32] N. Furukuyama and T.M. Rice, J. Phys. C **10**, L381 (1998); Phys. Rev. Lett. **81**, 3195 (1998).
[33] D.S. Dessau, Z.-X. Shen, D.M. King, D.S. Marshall, L.W. Lombardo, P.H. Dickinson, A.G. Loeser, J. DiCarlo, C.-H. Park, A. Kapitulnik, and W.E. Spicer, Phys. Rev. Lett. **71**, 2781 (1993).
[34] J.E. Hirsch and D.J. Scalapino, Phys. Rev. Lett. **56**, 2732 (1986).
[35] P.A. Lee and N. Read, Phys. Rev. Lett. **58**, 2691 (1987).
[36] M.J. Rice and S. Strässler, Solid State Commun. **13**, 125 (1973).
[37] C.J. Halboth and W. Metzner, Phys. Rev. B **61**, 7364 (2000).
[38] D. Zanchi and H.J. Schulz, Europhys. Lett. **44**, 235 (1998); Phys. Rev. B **61**, 13 609 (2000).
[39] Y.M. Vilk and A.-M.S. Tremblay, Europhys. Lett. **33**, 159 (1996); J. Phys. I **7**, 1309 (1997).
[40] J. Jackeli and V.Y. Yushankhai, Phys. Rev. B **56**, 3540 (1997).
[41] D. Menashe and B. Laikhtman, Phys. Rev. B **59**, 13 592 (1999).
[42] M.R. Norman, H. Ding, H. Fretwell, M. Randeria, and J.C. Campuzano, Phys. Rev. B **60**, 7585 (1999).
[43] H. Fukuyama and Y. Hasegawa, Prog. Theor. Phys. Suppl. **101**, 441 (1990); H. Fukuyama, Y. Hasegawa, and O. Narikiyo, J. Phys. Soc. Jpn. **60**, 2013 (1991).
[44] J.R. Engelbrecht and M. Randeria, Phys. Rev. Lett. **65**, 1032 (1990); Phys. Rev. B **45**, 12 419 (1992).
[45] C.N. Yang, Phys. Rev. Lett. **63**, 2144 (1989).
[46] E. Demler and S-C. Zhang, Phys. Rev. Lett. **75**, 4126 (1995).
[47] R.S. Markiewicz, J. Phys. C **2**, 665 (1990).
[48] D.M. Newns, P.C. Pattnaik, and C.C. Tsuei, Phys. Rev. B **43**, 3075 (1991).